Supplementary Information

Reinforced and superinsulating silica aerogel through in situ cross-linking with silane terminated prepolymers

Subramaniam Iswar, Geert M. B. F. Snellings, Shanyu Zhao, Rolf Erni, Yeon Kyoung Bahk, Jing Wang, Marco Lattuada, Matthias M. Koebel and Wim J. Malfait

Table of contents

1. Preparation and characterization of prepolymers from natural oil based polyols

Five silane terminated prepolymers, namely Empa 1990, Empa 2033, Empa D-140, Empa D-265 and Empa D-290, were synthesized by using Natural Oil based Polyols (NOPs) namely Radianol 1990 (Oleon), Pripol^{TM} 2033 (Croda), Polycin® D-140, Polycin® D-265 and Polycin® D-290 (Vertellus®) respectively. Following is the general experimental procedure:

- Start with a calculated amount of the respective polyol in a beaker at room temperature.
- Add catalyst (Fomrez® UL-28) dropwise under continuous stirring.
- In a next step, add the calculated amount of 3-(triethoxysilyl) propyl isocyanate (Sigma-Aldrich) dropwise via a separation funnel under continuous stirring.
- Temperature is monitored during the reaction to determine the exotherm.
- No solvent is used during the reaction.

After the prepolymers were synthesized, they were characterized by solution ^{1}H NMR. For all prepolymers from the various NOPs, the reaction is complete as evidenced by the disappearance of e band and the appearance of f' and e' bands (Figure S1). The peak intensity ratio f', b' and e' is very close to 2-6-2 protons for all samples, indicating there is exactly one urethane bond per silane group as expected.

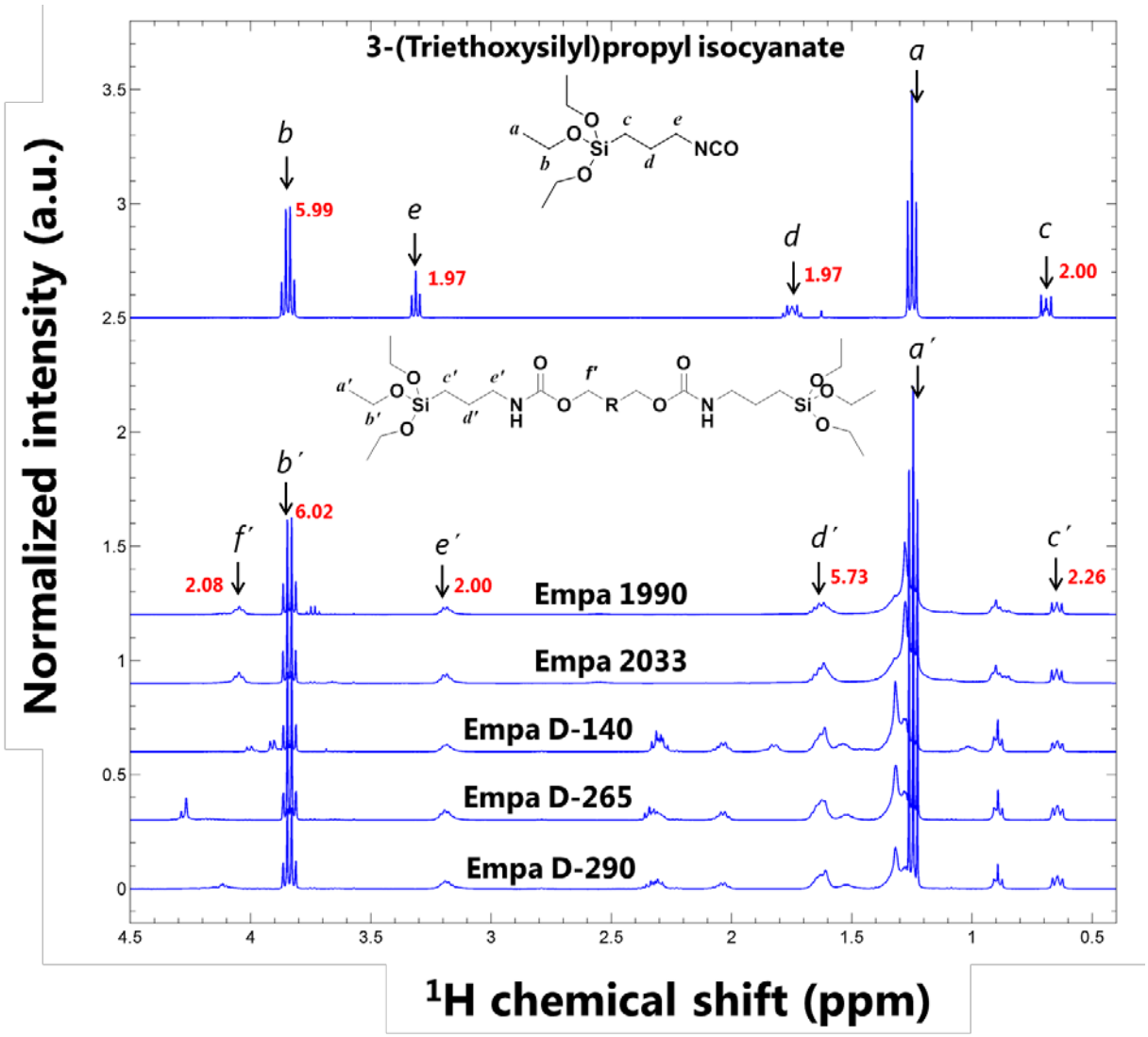

Figure S1. ^{1}H NMR of five silane terminated prepolymers namely Empa 1990, Empa 2033, Empa D-140, Empa D-265 and Empa D-290 synthesized by using Natural Oil based Polyols (NOPs).

2. Thermal conductivity setup

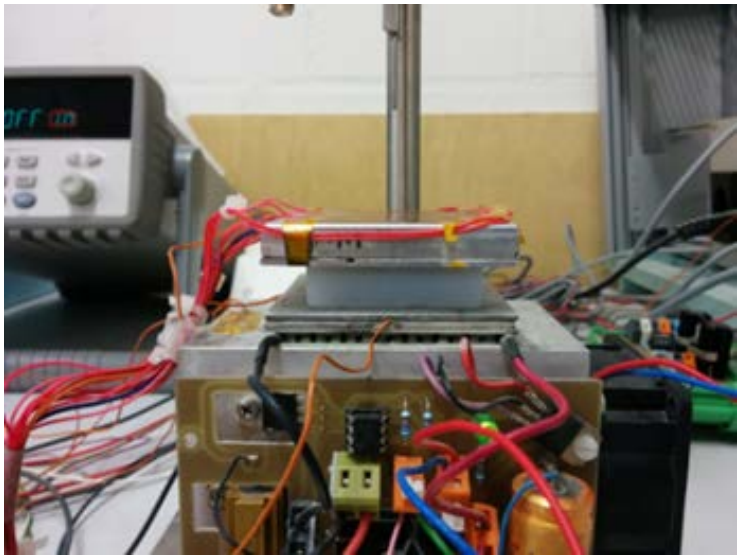

Figure S2. Custom built guarded hot plate device for thermal conductivity measurement[1].

3. Particle release by the mechanical impact setup

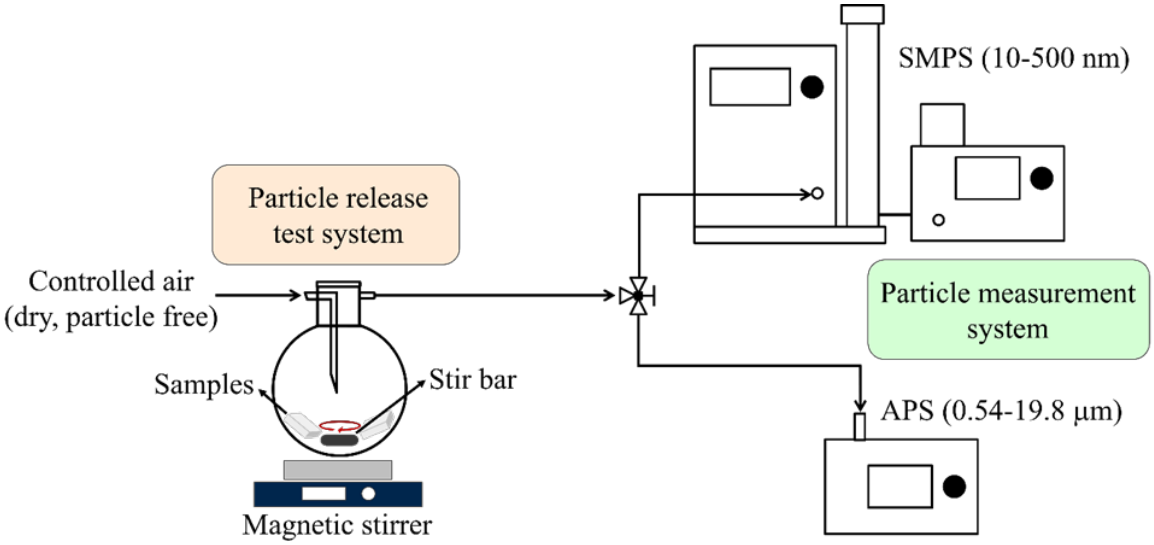

Figure S3. Experimental setup for the particle release from aerogels by the mechanical impact.

4. Digital photos

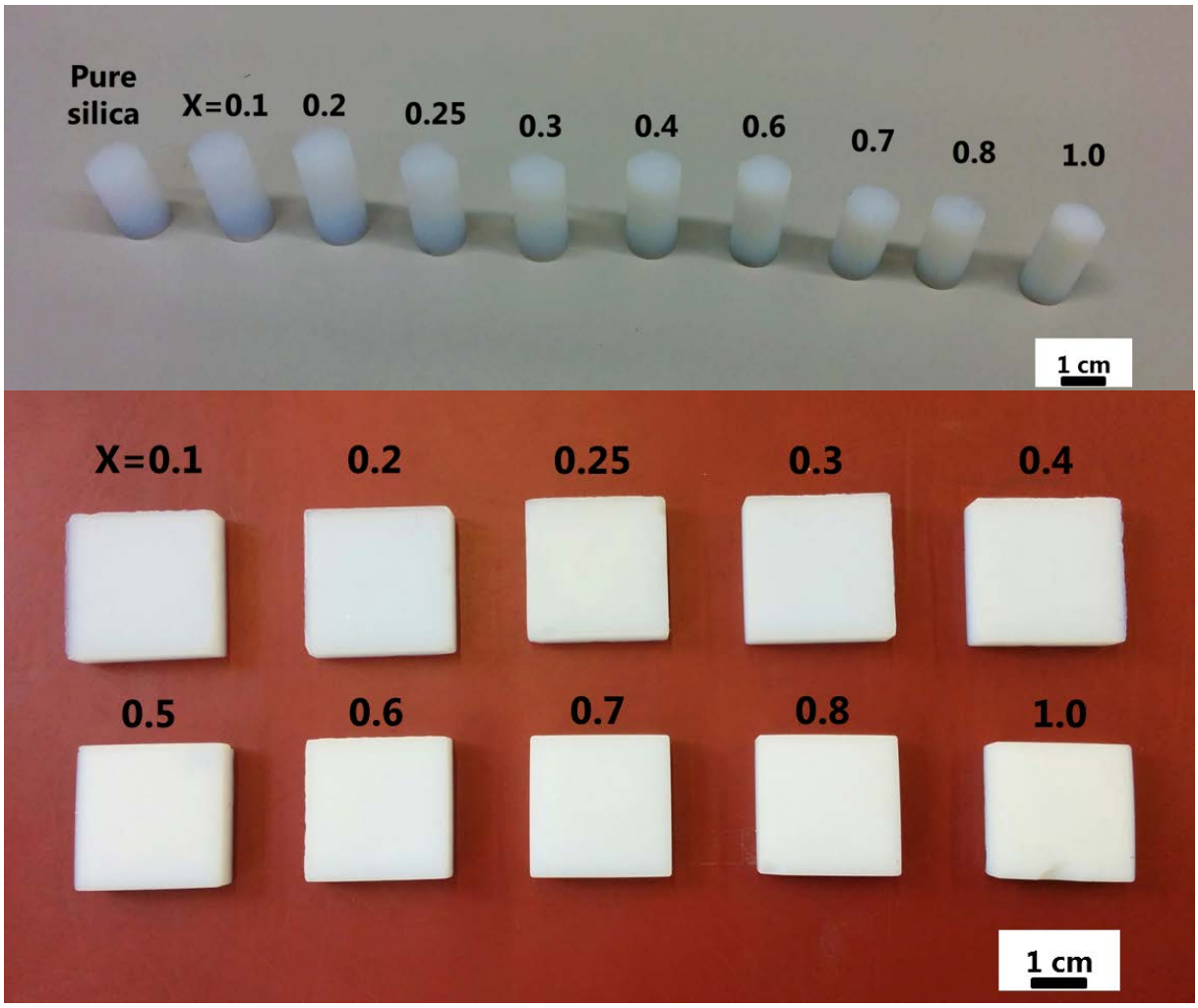

Figure S4. Digital photos of pure reference silica and EP-M 95 hybrid aerogels for different concentrations (prepolymer (X):SiO_2).

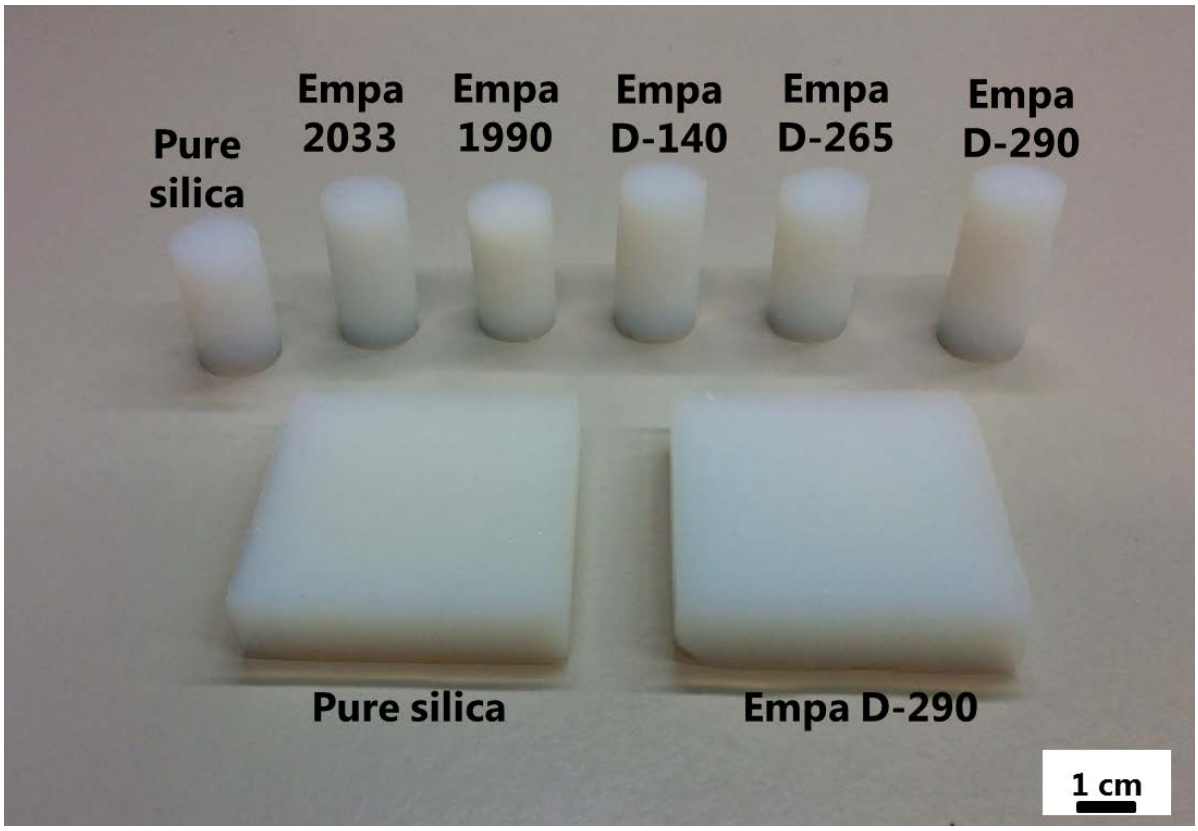

Figure S5. Digital photos of pure reference silica and NOP based hybrid aerogels for X=0.3 (prepolymer (X):SiO_2).

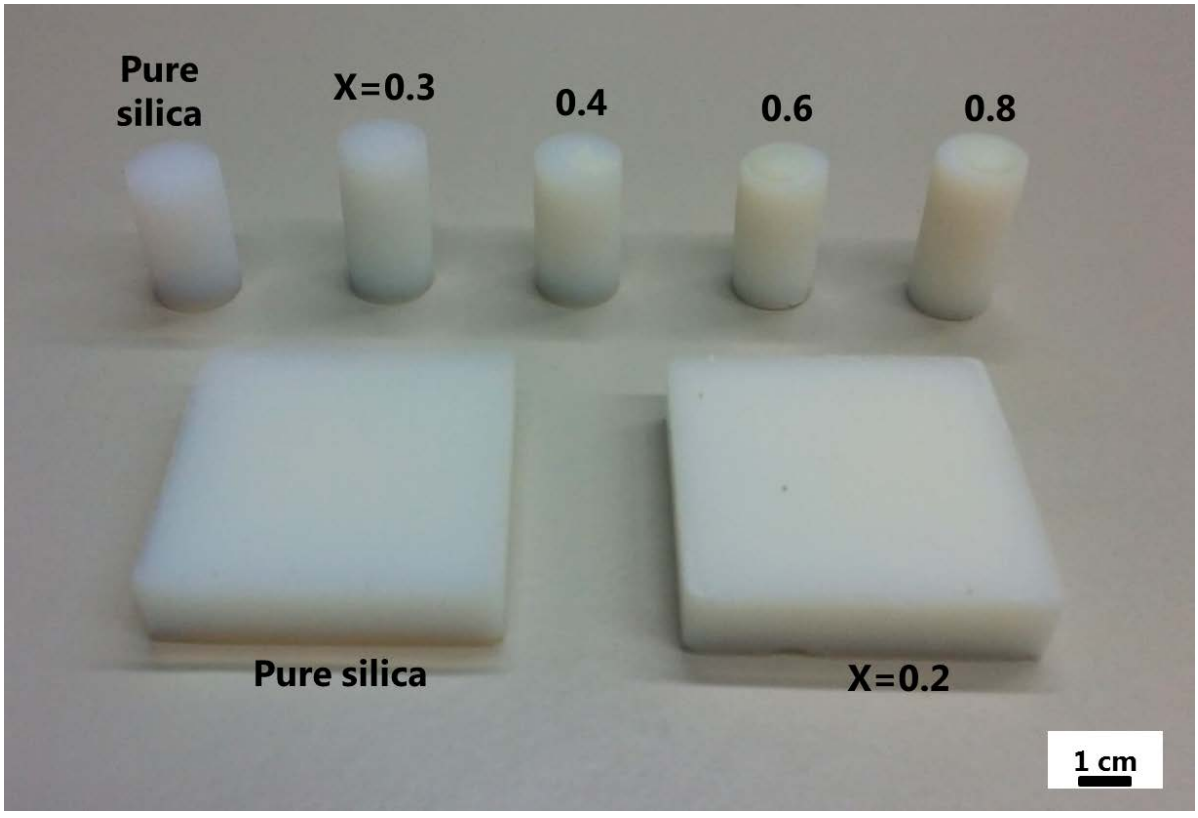

Figure S6. Digital photos of pure reference silica and Empa 2033 hybrid aerogels for different concentrations (prepolymer (X):SiO_2).

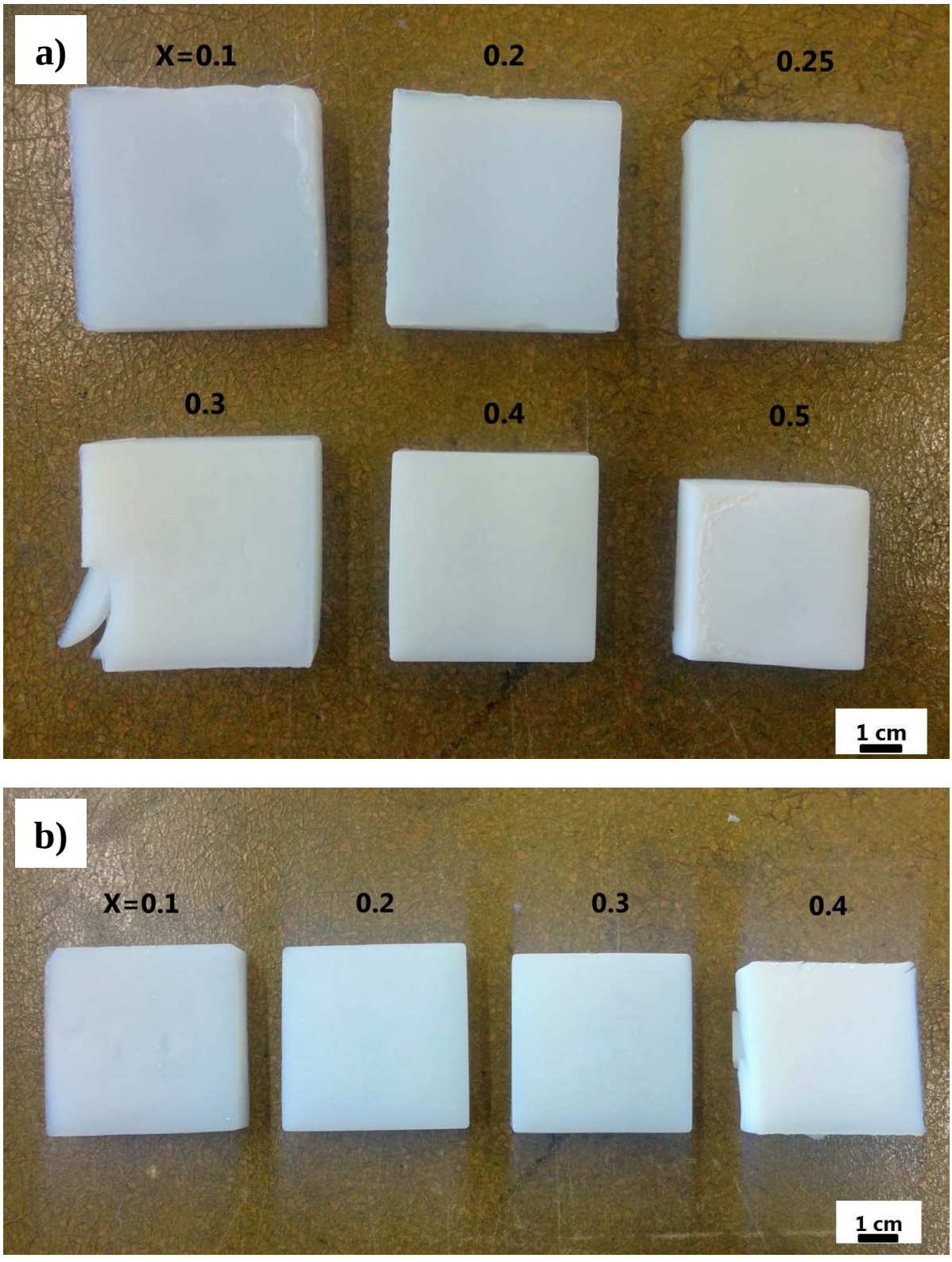

Figure S7. Digital photos of (a) STP-E 15 and (b) STP-E 35 hybrid aerogels for different concentrations (prepolymer (X):SiO_2).

5. Density and thermal conductivity

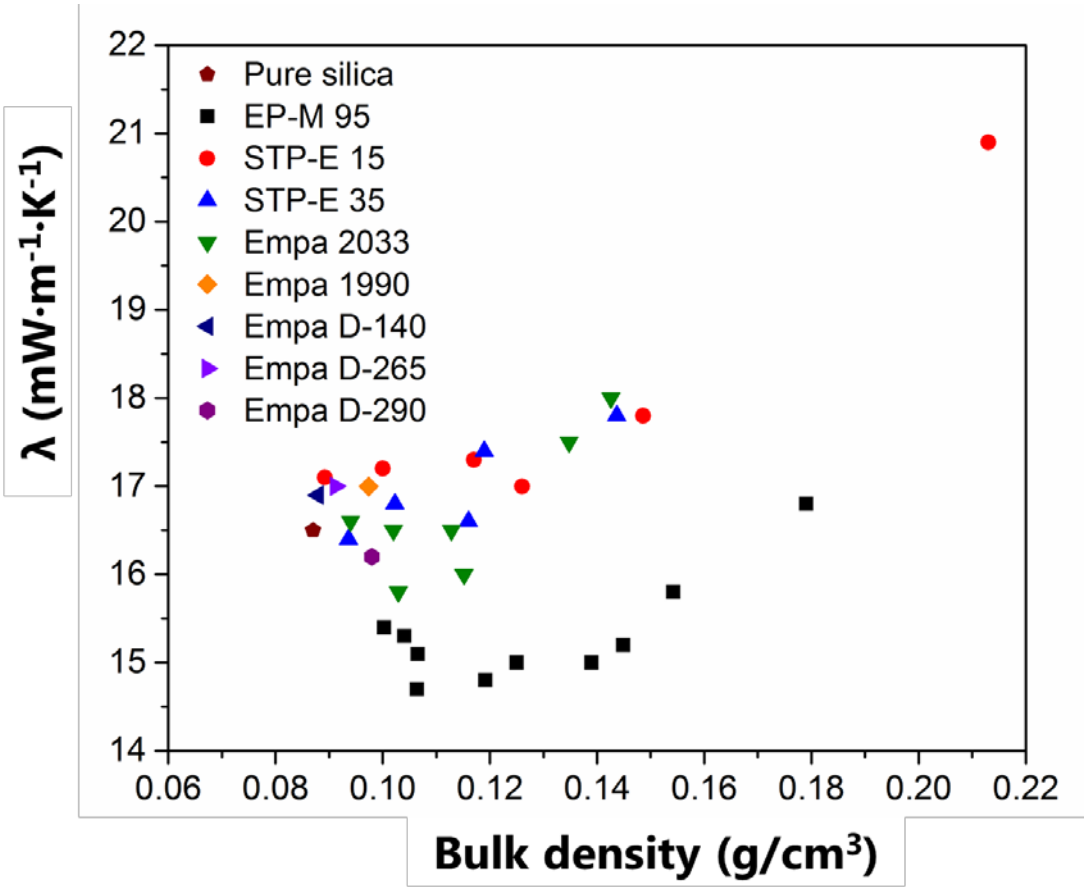

Figure S8. Thermal conductivity as a function of density of hybrid aerogels using different prepolymers.

6. NMR Spectroscopy

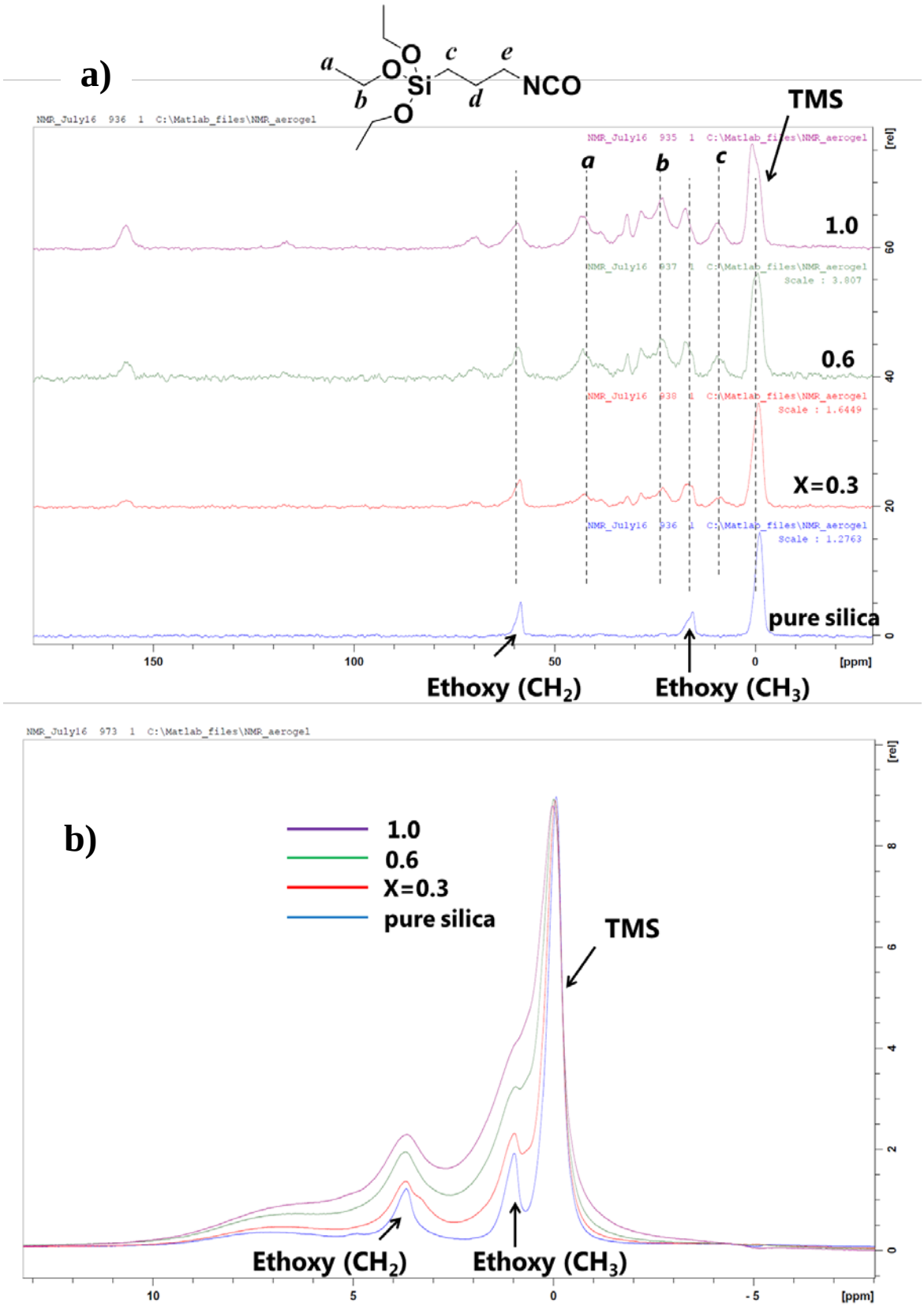

Figure S9. (a) ^{1}H-^{13}C cross polarization (CP) and (b) Quantitative ^{1}H solid–state MAS NMR spectra of EP-M 95 hybrid aerogels for increasing concentrations.

7. FTIR Spectroscopy

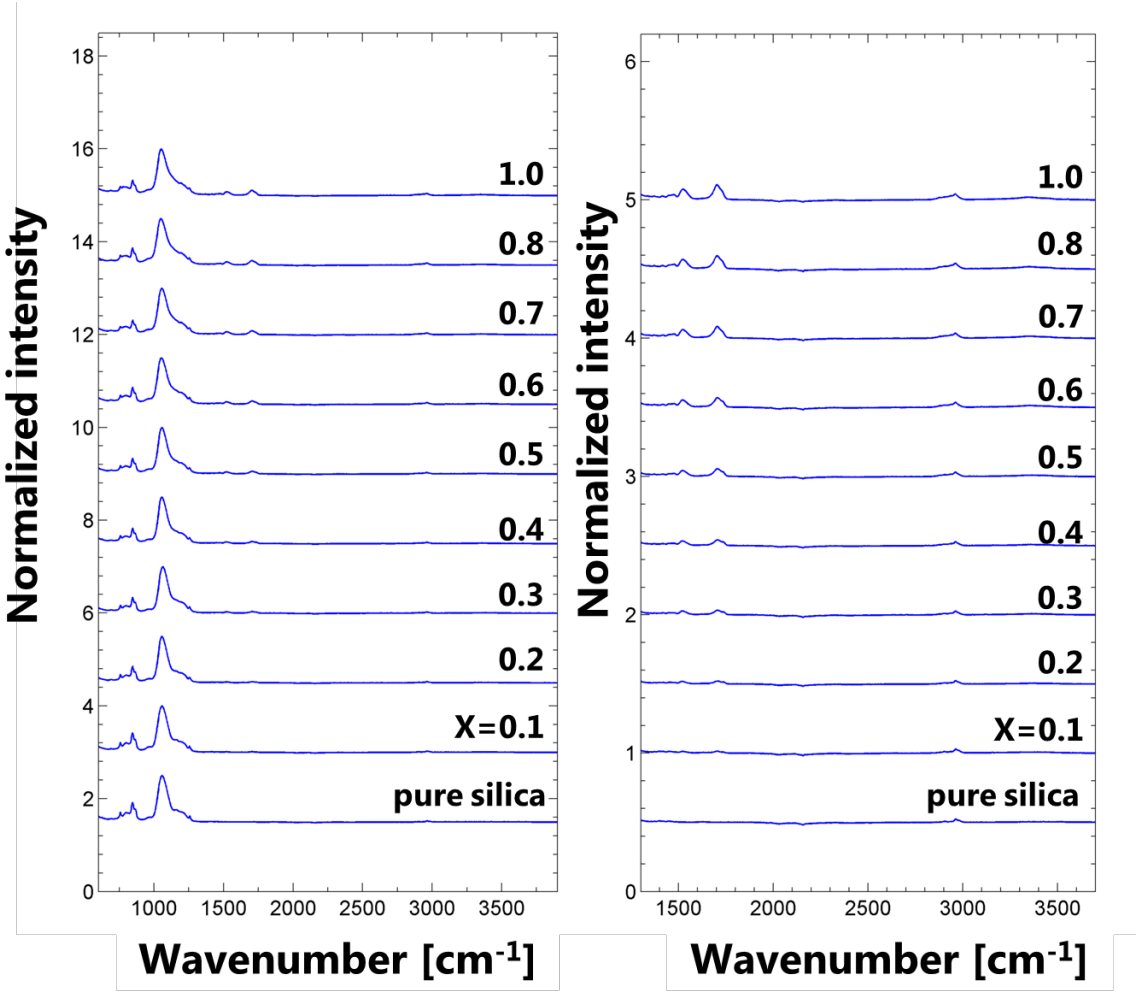

Figure S10. ATR-FTIR spectra of pure reference silica and EP-M 95 hybrid aerogels for increasing concentrations.

ATR-FTIR spectra of EP-M 95 hybrid aerogels display changes with increasing concentrations when compared to pure reference silica aerogel, with an increase in the broad bands near 2960 cm^{-1} related to the C-H stretching vibration and the increasing intensity of C-N, N-H stretching bands near 1520 cm^{-1} and C=O bands near 1700 cm^{-1} respectively[2,3] (Figure S10). The increasing intensities of these bands confirm the systematic incorporation of the prepolymer into the aerogel matrix.

The higher variability in the prepolymer peak intensities for the X=1.0 sample, compared to those with lower prepolymer concentrations, is indicative of an inhomogeneity in the prepolymer distribution (Figure S11).

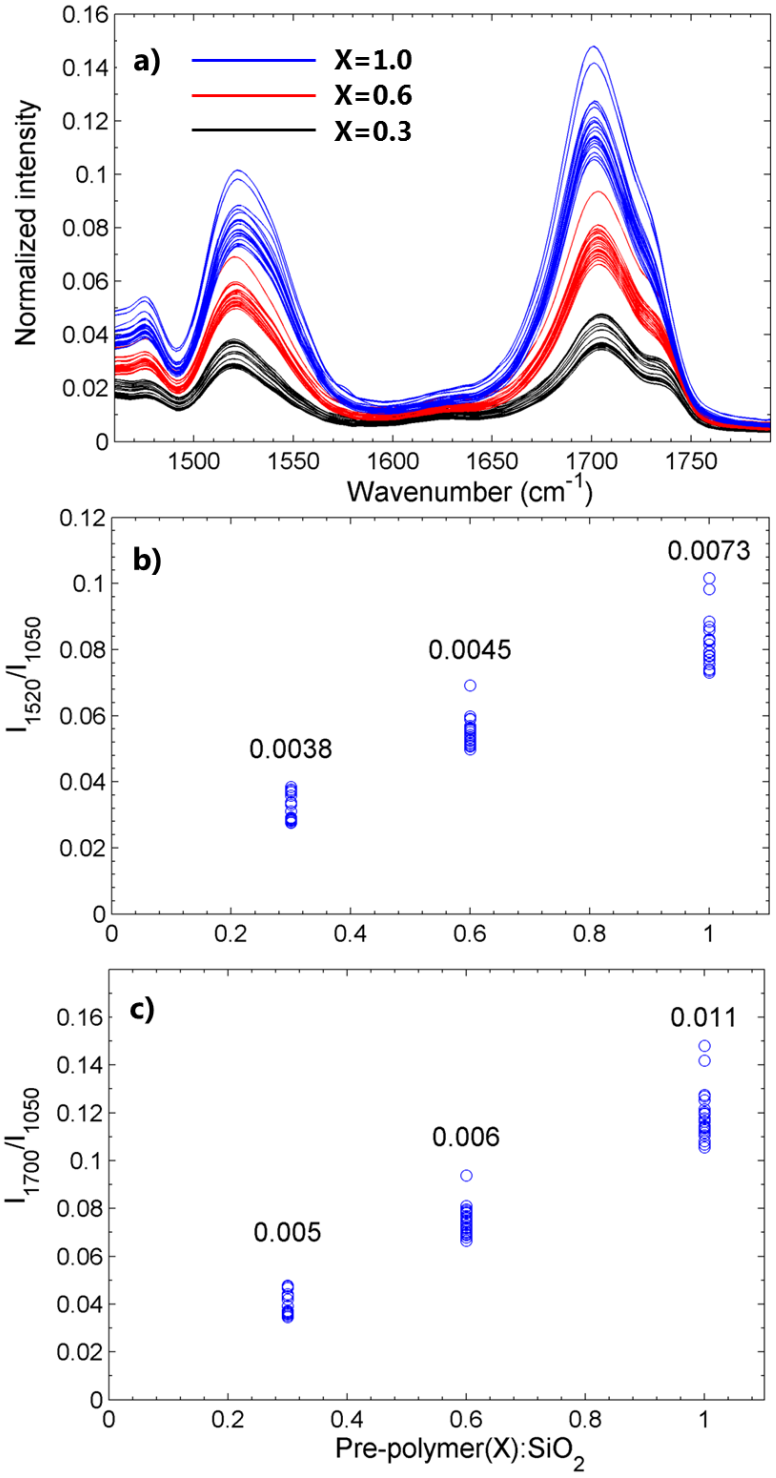

Figure S11. (a) ATR-FTIR spectra; Maximum peak intensities at (b) 1520 cm^{-1} and (c) 1700 cm^{-1} of EP-M 95 hybrid aerogels for increasing concentrations. The numbers indicate the standard deviation from 21 measurements.

8. Elemental analysis

Table S1: Elemental analysis of pure reference silica and hybrid aerogels.

Sample	Carbon (%)	Hydrogen (%)	Nitrogen (%)
Pure reference silica (X=0.0)	13.83 ± 1.0	3.40 ± 0.5	0.05 ± 0.04
EP-M 95 (X=0.3)	18.81 ± 1.0	4.02 ± 0.5	1.09 ± 0.04
EP-M 95 (X=0.6)	22.31 ± 1.0	4.35 ± 0.5	1.76 ± 0.04
EP-M 95 (X=1.0)	26.17 ± 1.0	4.75 ± 0.5	2.42 ± 0.04
STP-E 15 (X=0.3)	14.86 ± 1.0	3.35 ± 0.5	0.12 ± 0.04
STP-E 35 (X=0.3)	14.76 ± 1.0	3.34 ± 0.5	0.14 ± 0.04
Empa 2033 (X=0.3)	18.26 ± 1.0	3.85 ± 0.5	0.35 ± 0.04

The uncertainties correspond to one standard deviation from 3 repeat measurements.

9. Scanning and transmission electron microscopy analysis

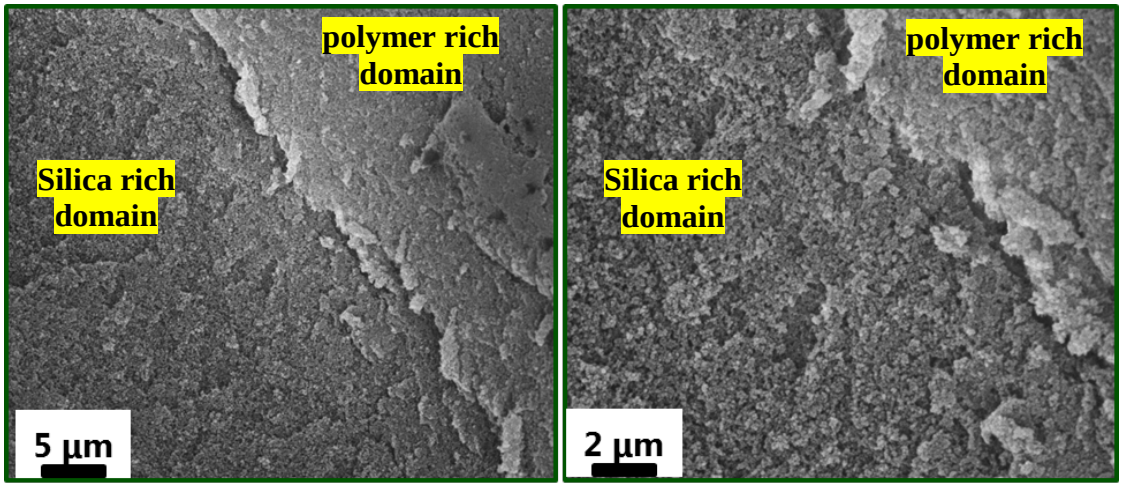

Figure S12. SEM images of EP-M 95 hybrid aerogel for X=1.0 concentration.

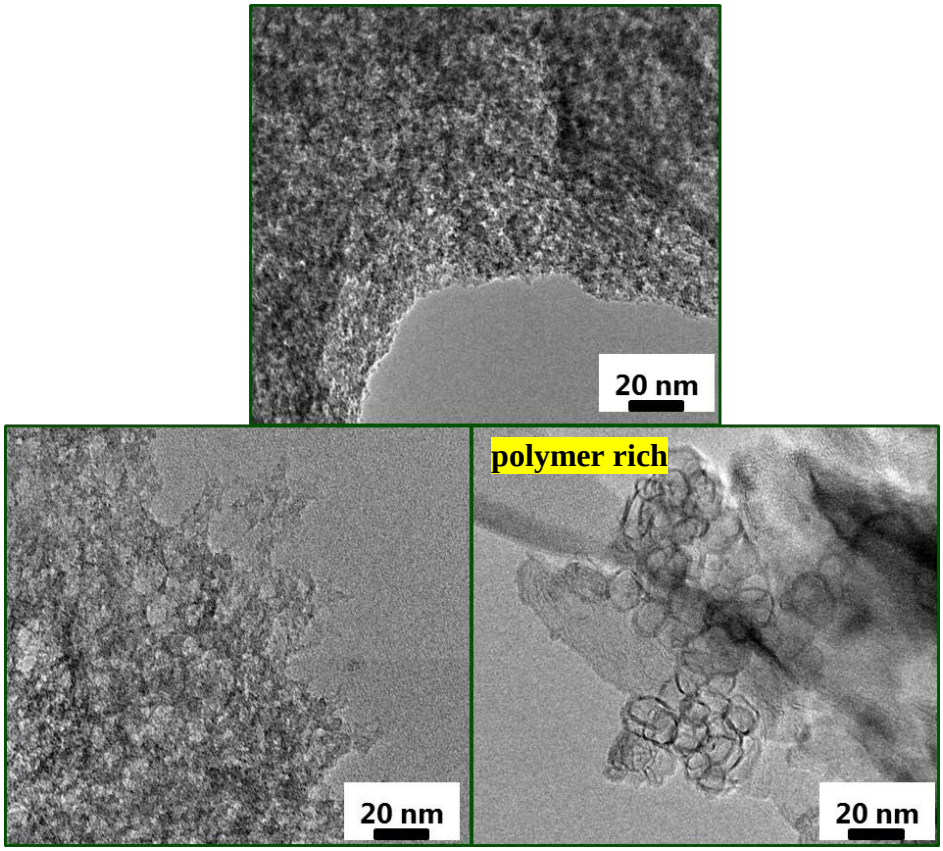

Figure S13. TEM images of EP-M 95 hybrid aerogel for X=1.0 concentration.

There are inhomogenity in the microstructure for EP-M 95 hybrid aerogel at X=1.0 concentration as depicted in the SEM and TEM images due to the presence of silica rich and polymer rich domains (Figs. S12 and S13).

10. Nitrogen adsorption-desorption characterization

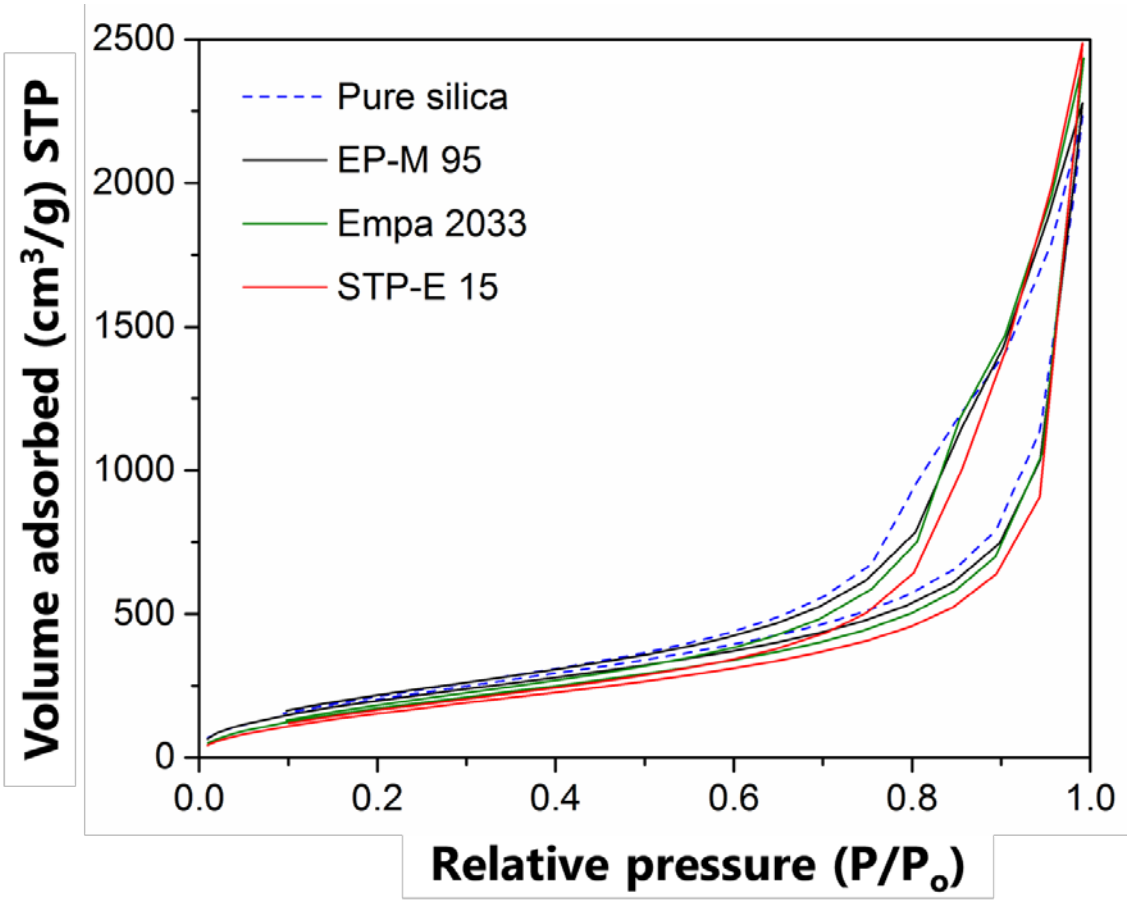

Figure S14. Nitrogen sorption isotherms of pure reference silica aerogel and EP-M 95, Empa 2033, STP-E 15 hybrid aerogels for X=0.3 concentration.

11. Uniaxial compression test

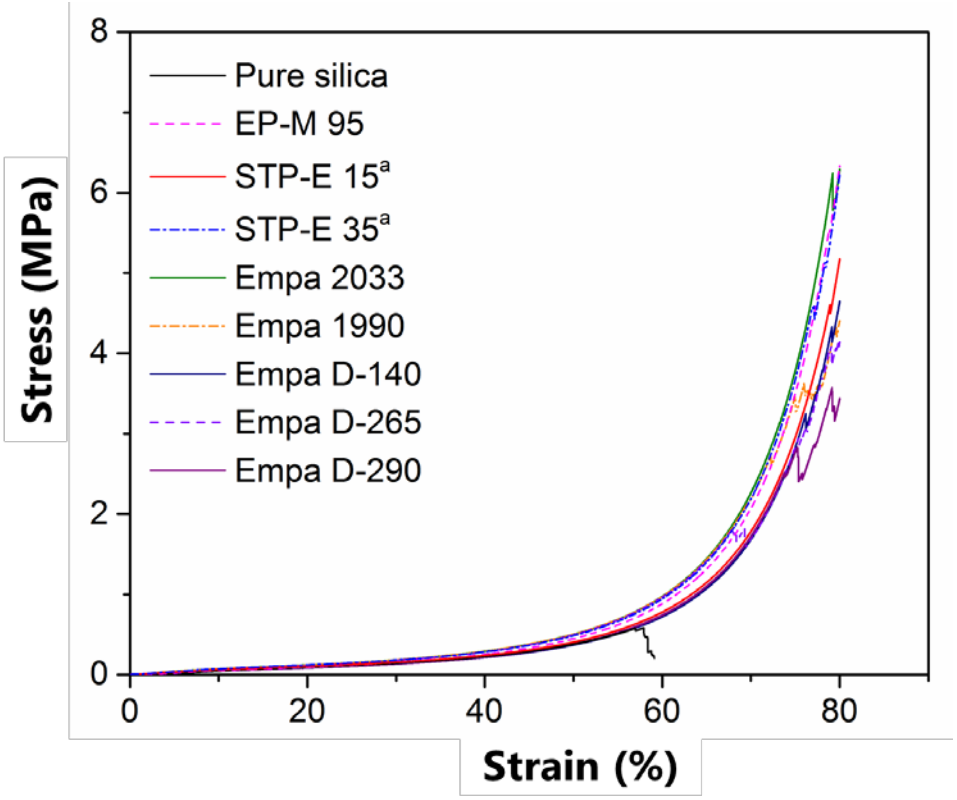

Figure S15. Compressive stress-strain curves of pure reference silica and hybrid aerogels from different prepolymers for X=0.3 concentration; [a] for X=0.25 (X:SiO_2).

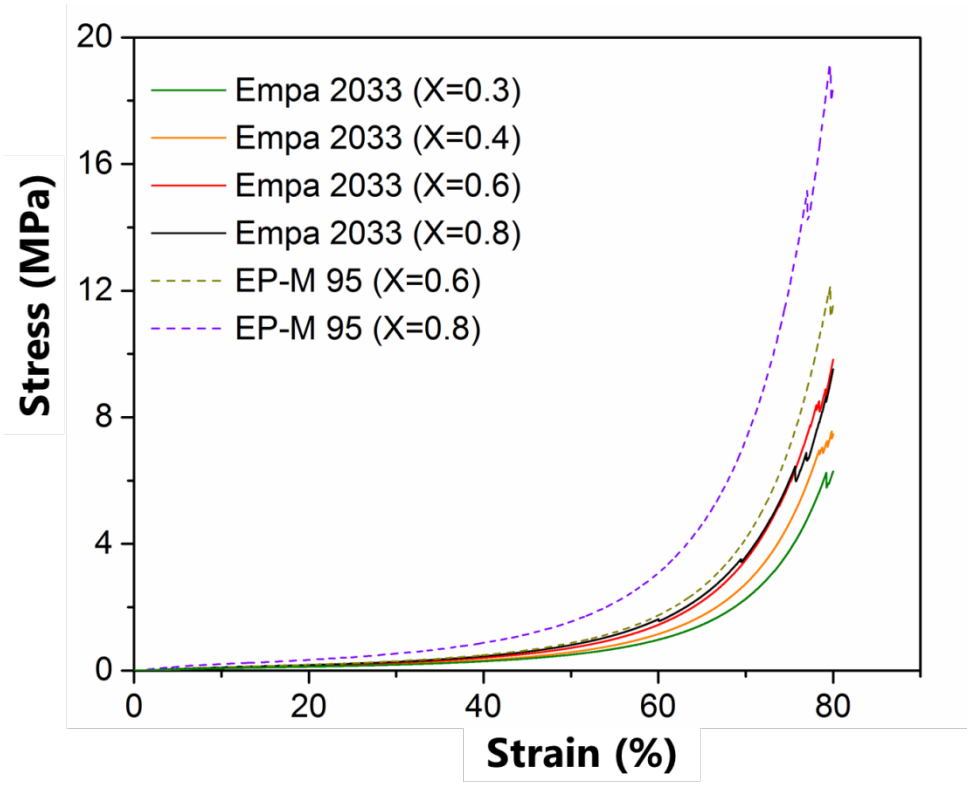

Figure S16. Compressive stress-strain curves of Empa 2033 hybrid aerogels for increasing concentrations.

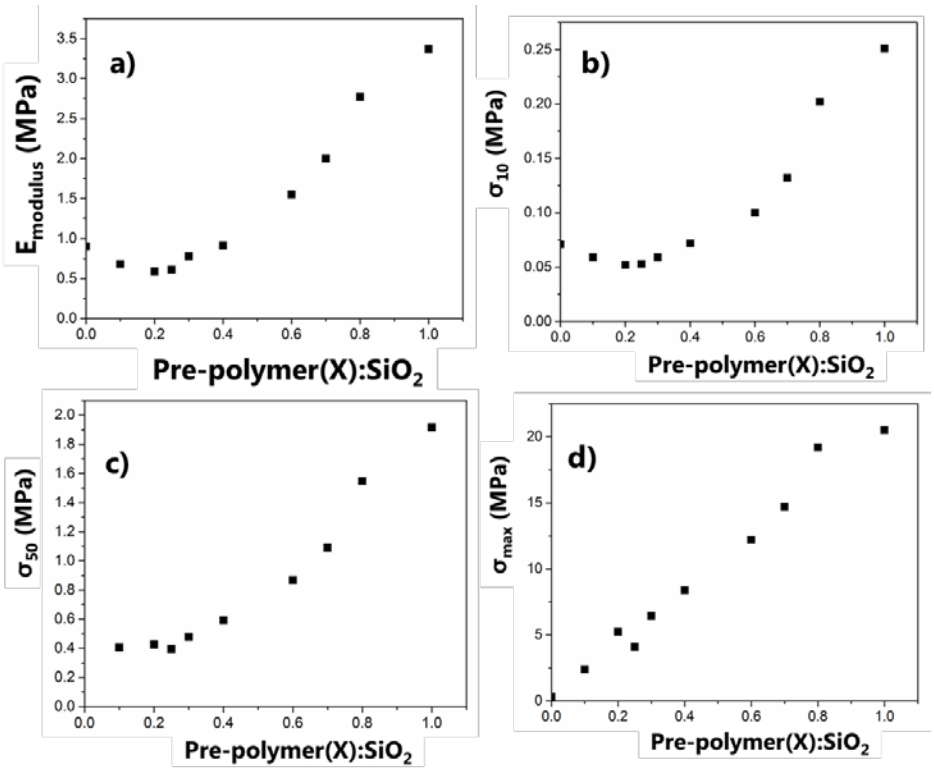

Figure S17. (a) Compressive modulus (E), (b) Compressive strength at 10% strain (σ_{10}), (c) Compressive strength at 50% strain (σ_{50}) and (d) Final compressive strength (σ_{max}) of EP-M 95 hybrid aerogels for increasing concentrations.

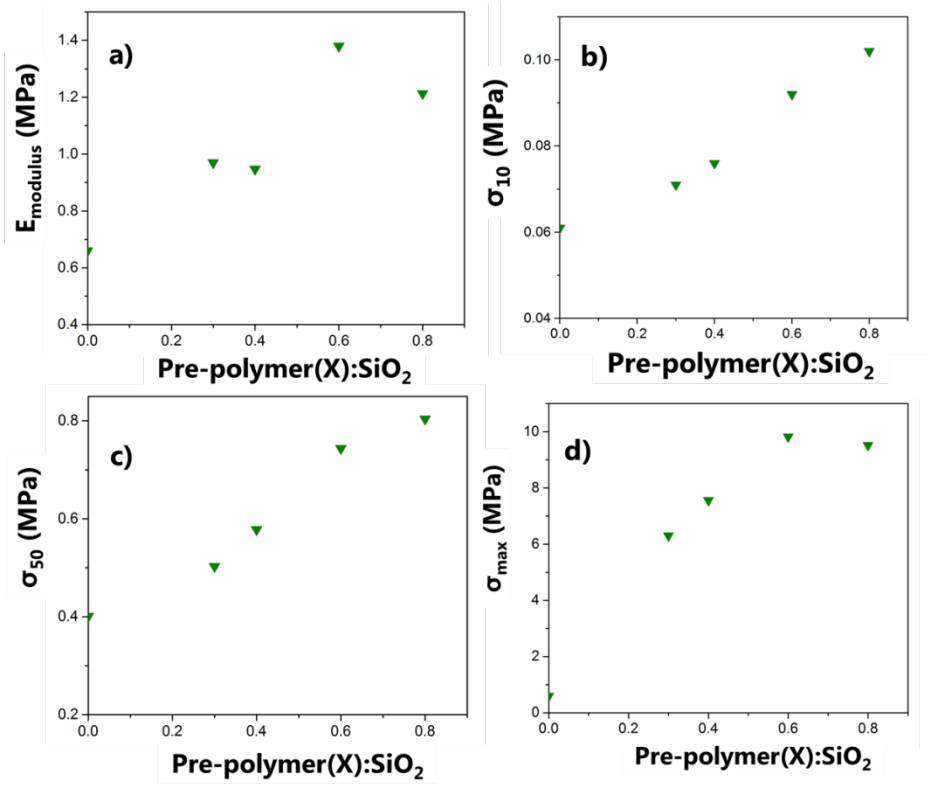

Figure S18. (a) Compressive modulus (E), (b) Compressive strength at 10% strain (σ_{10}), (c) Compressive strength at 50% strain (σ_{50}) and (d) Final compressive strength (σ_{max}) of Empa 2033 hybrid aerogels for increasing concentrations.

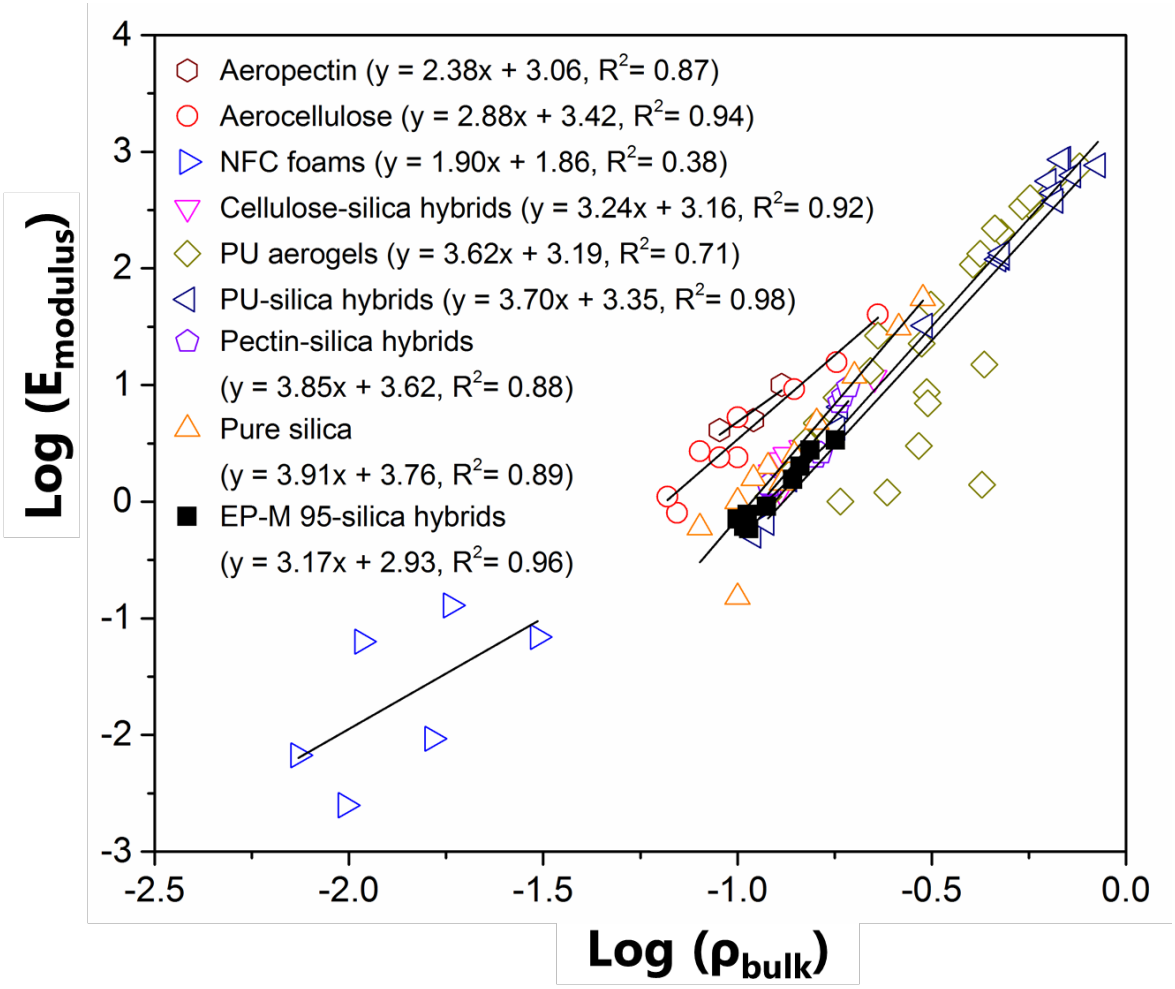

Figure S19. Log ($E_{modulus}$) vs Log (bulk density) for different aerogel like materials[4–16].

Table S2: Slopes of Log ($E_{modulus}$) vs Log (bulk density) for different aerogel like materials[4–16]

Samples	Slope
Aeropectin	2.38
Aerocellulose	2.88
NFC foams	1.90
Cellulose-silica hybrids	3.24
PU aerogels	3.62
PU-silica hybrids	3.70
Pectin-silica hybrids	3.85
Pure reference silica	3.91
EP-M 95-silica hybrids	3.17

12. Particle release results

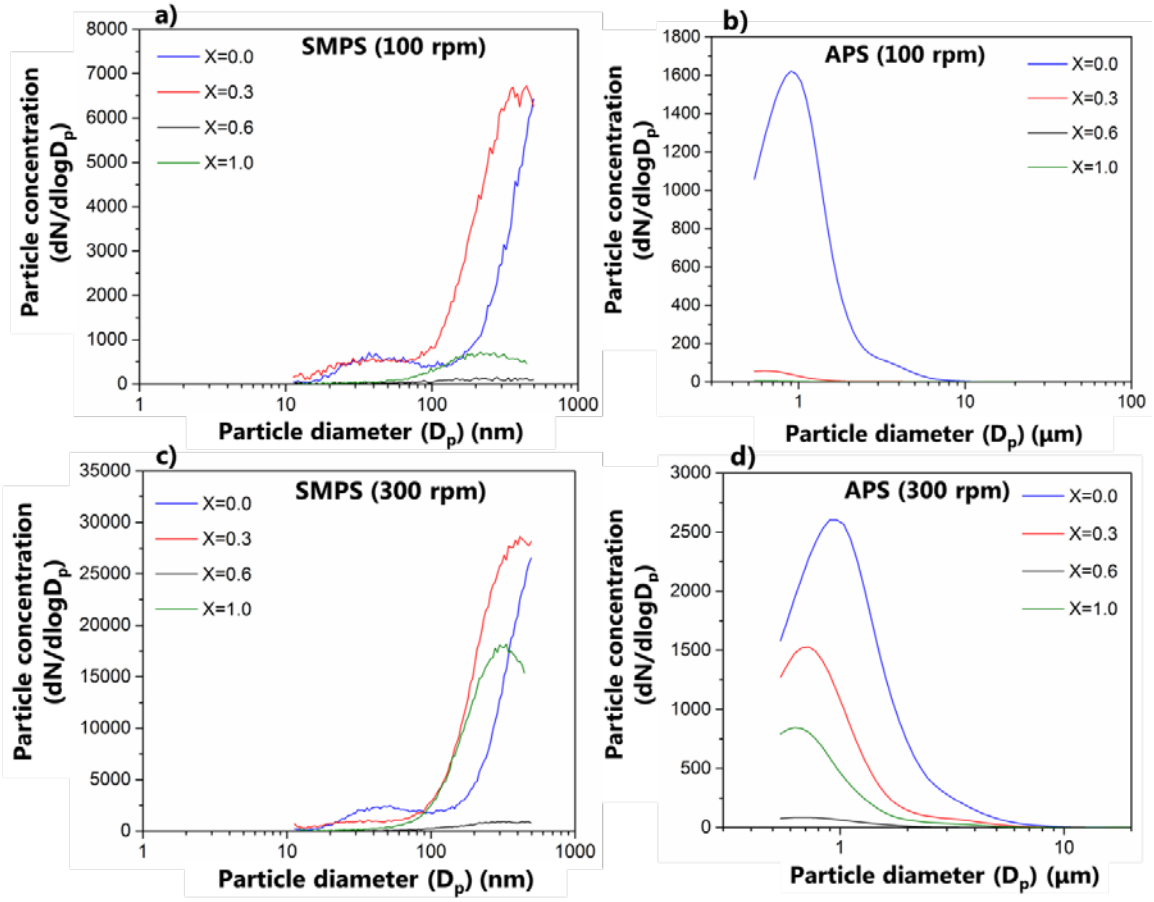

Figure S20. Particle release at 100 rpm for (a) SMPS (10-500 nm), (b) APS (0.54-19.8 µm) and at 300 rpm for (c) SMPS (10-500 nm), (d) APS (0.54-19.8 µm) of EP-M 95 hybrid aerogels for different concentrations.

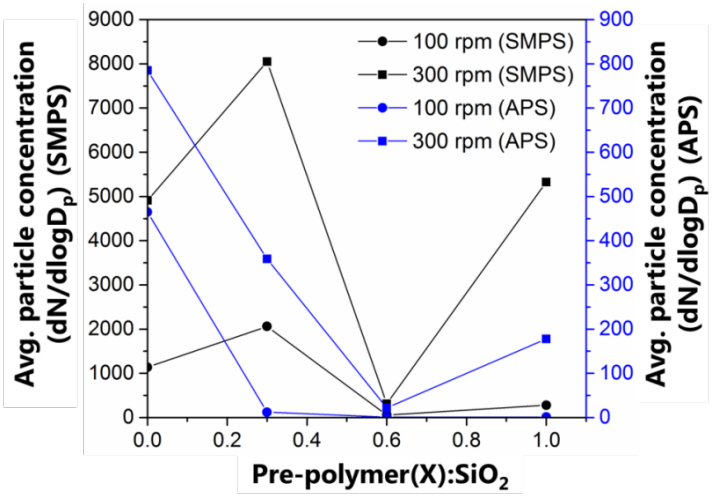

Figure S21. Average particle concentration of EP-M 95 hybrid aerogels measured for 1 hour at different concentrations for SMPS (10-500 nm) and APS (0.54-19.8 µm) respectively.

When compared to pure reference silica aerogel, the average particle concentration went down significantly for the EP-M 95 hybrid aerogels with increasing concentrations. Mechanically strong hybrid aerogels reduced the particle release (SMPS (10-500 nm), APS (0.54-19.8 μm)) observed for both mild (100 rpm) and extreme mechanical impact conditions (300 rpm) (Figs. S20a-d and S21). The increase in the particle release for the hybrid aerogels at 1.0 concentration can be related to the inhomogeneity in the microstructure due to the silica rich and polymer rich domains as observed in the SEM, TEM and water contact angle analysis (Figs. S12, S13 and S27) and the variations in the surface inhomogeneity as indicated by the ATR-FTIR analysis (Figure S11).

13. Differential thermogravimetric analysis

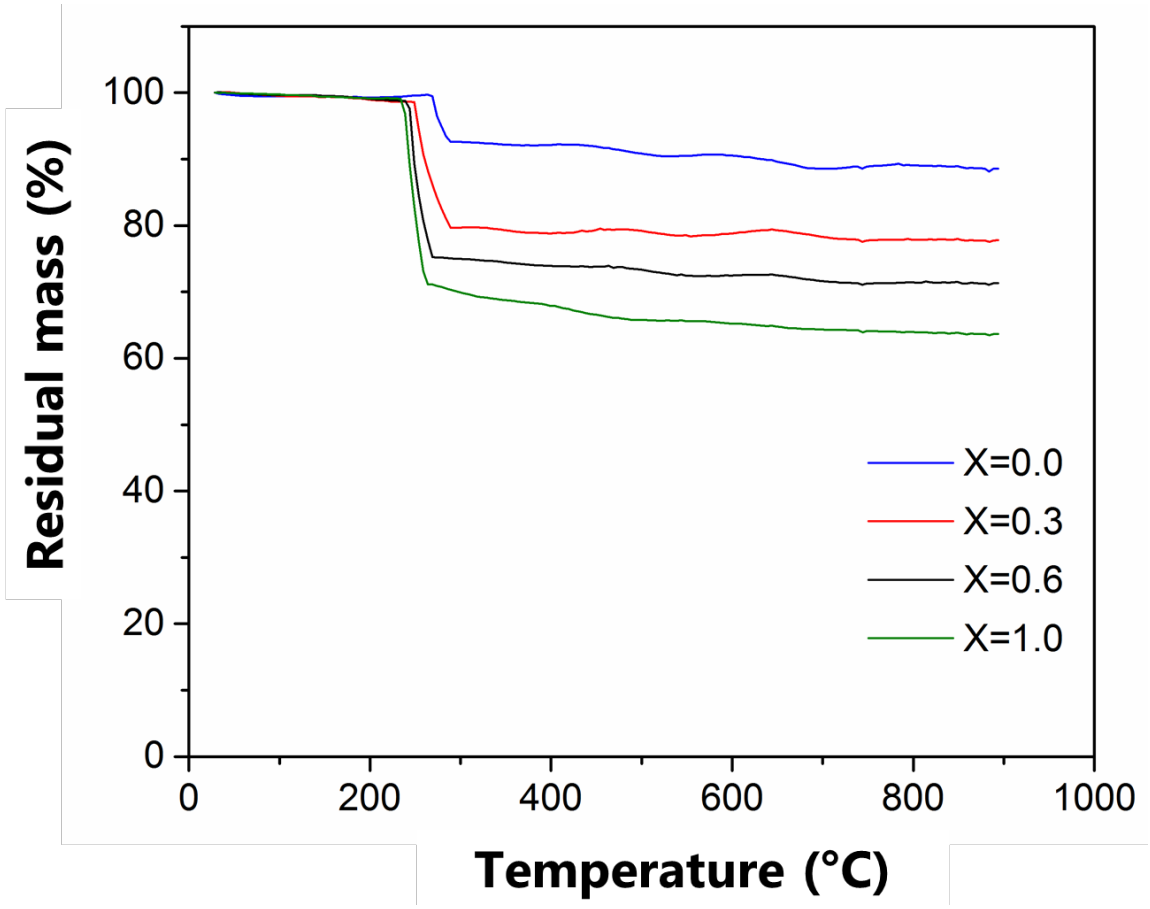

Figure S22. TGA curves (in 80% v/v oxygen and 20% v/v nitrogen) of pure reference silica aerogel (X=0.0) and EP-M 95 hybrid aerogels for different concentrations.

Figure S22 shows the thermogravimetric analysis (TGA) of pure reference silica aerogel (X=0.0) and EP-M 95 hybrid aerogels for different concentrations in the temperature range of 30-900°C in air at a heating rate of 5°C/min. For all samples, there is minimal weight loss of about 1% up to 200°C. Pure reference silica aerogel starts to decompose at 274°C due to the loss of trimethylsilyl (TMS) groups present on the silica aerogel backbone as reported in the literature[17,18]. They show the lowest weight loss of 11.8% compared to the EP-M 95 hybrid aerogels. On the other hand, the hybrid aerogels (with increasing concentrations) start to decompose between 245-262°C with a weight loss between 22 to 36%. Hence, an operating temperature above 240°C is not recommended for the EP-M 95 hybrid aerogels.

14. Humidity uptake

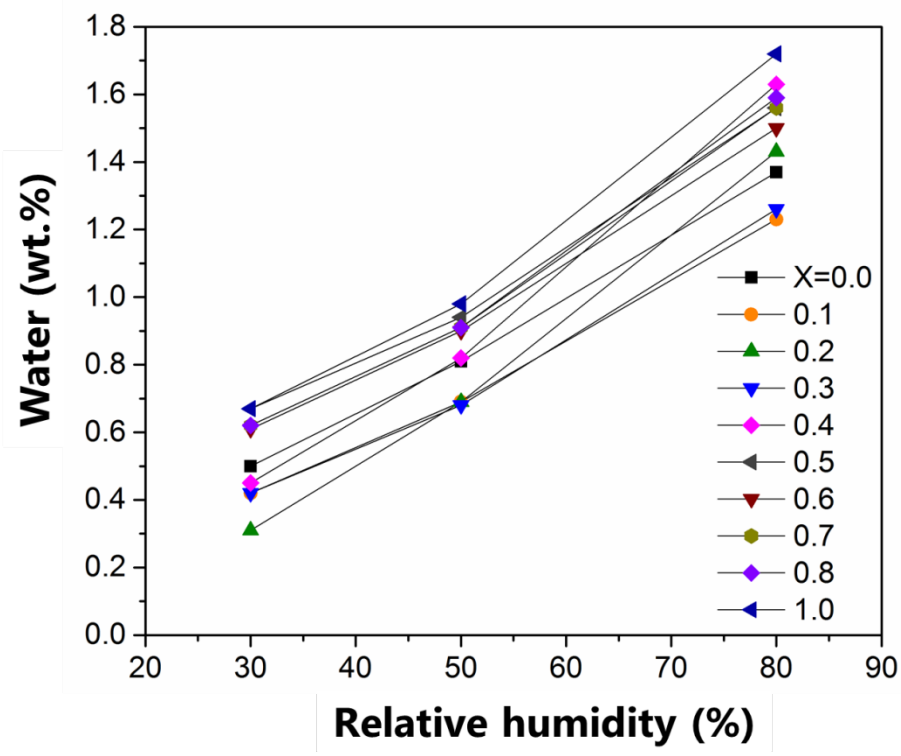

Figure S23. Humidity uptake of pure reference silica and EP-M 95 hybrid aerogels as a function of relative humidity for different concentrations.

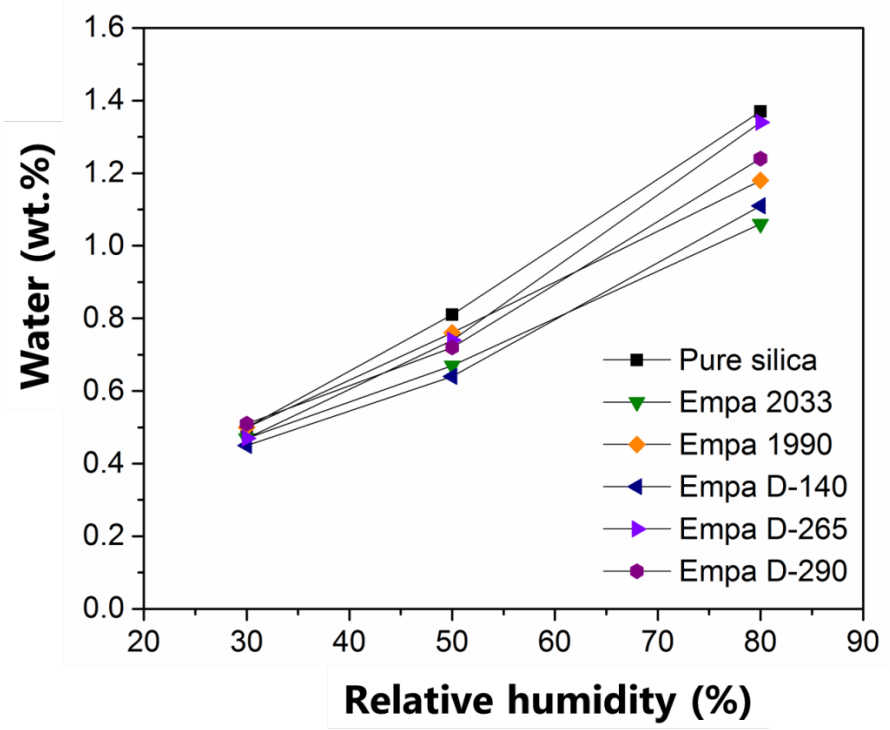

Figure S24. Humidity uptake of Natural Oil based Polyol (NOP) based hybrid aerogels as a function of relative humidity for X=0.3 concentration.

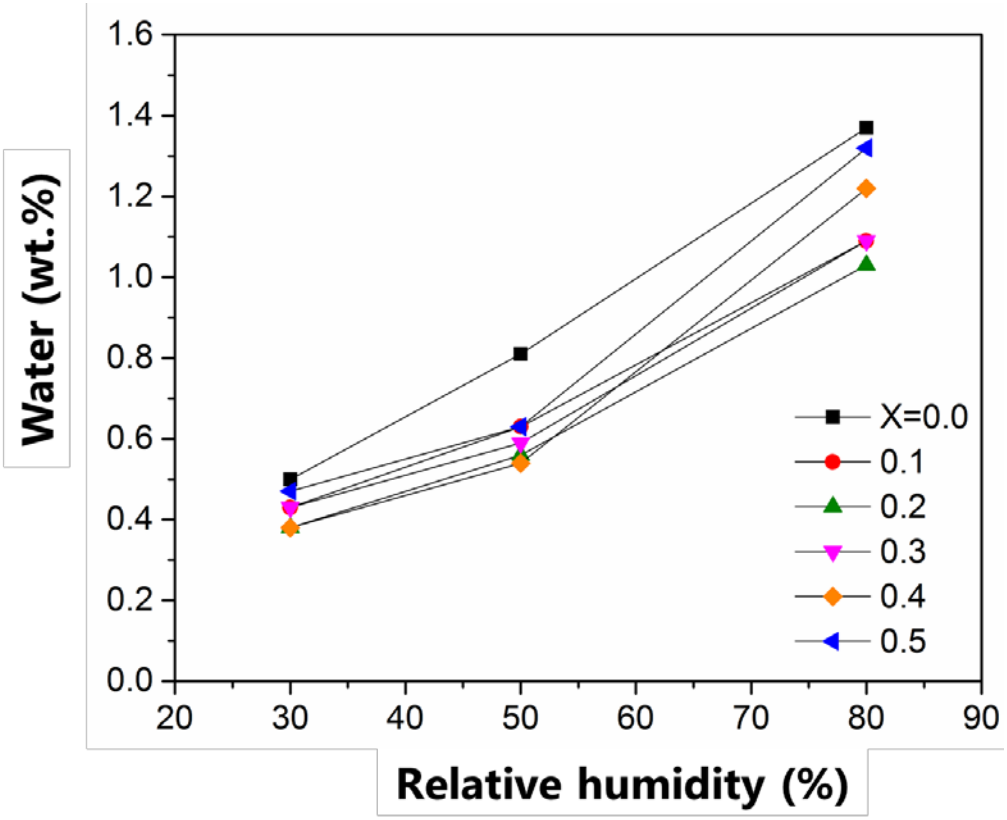

Figure S25. Humidity uptake of pure reference silica and STP-E 15 hybrid aerogels as a function of relative humidity for different concentrations.

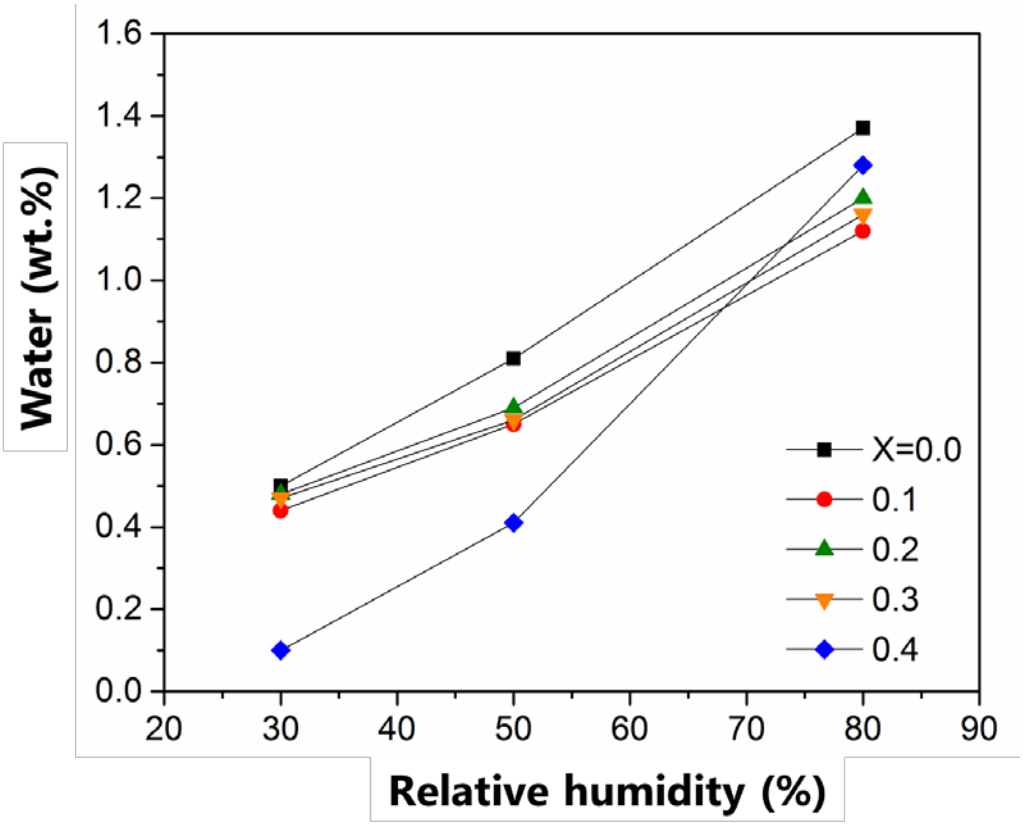

Figure S26. Humidity uptake of pure reference silica and STP-E 35 hybrid aerogels as a function of relative humidity for different concentrations.

15. Water contact angle

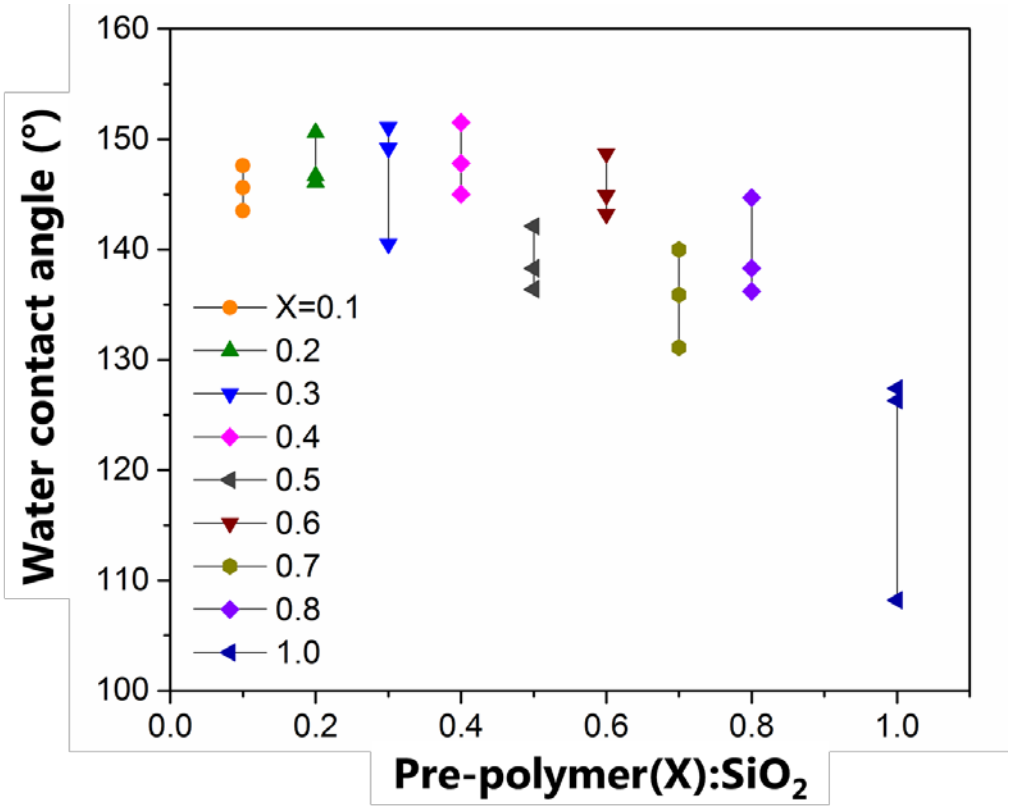

Figure S27. Water contact angles of EP-M 95 hybrid aerogels for increasing concentrations.

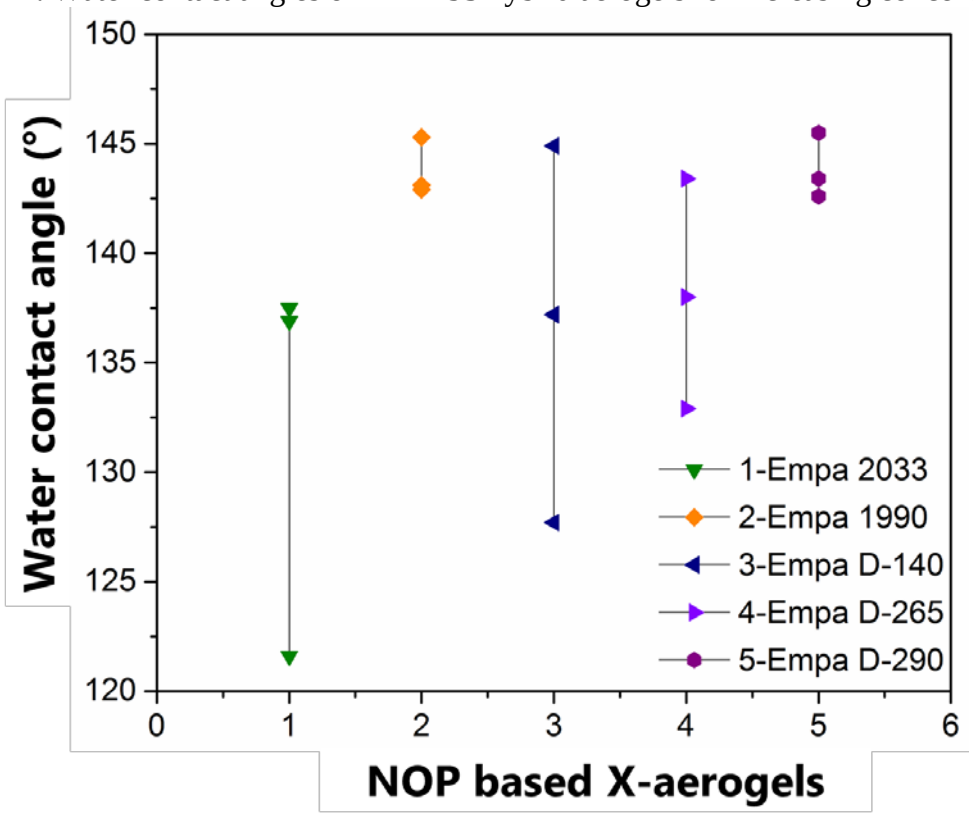

Figure S28. Water contact angles of Natural Oil based Polyol (NOP) based hybrid aerogels for X=0.3 concentration.

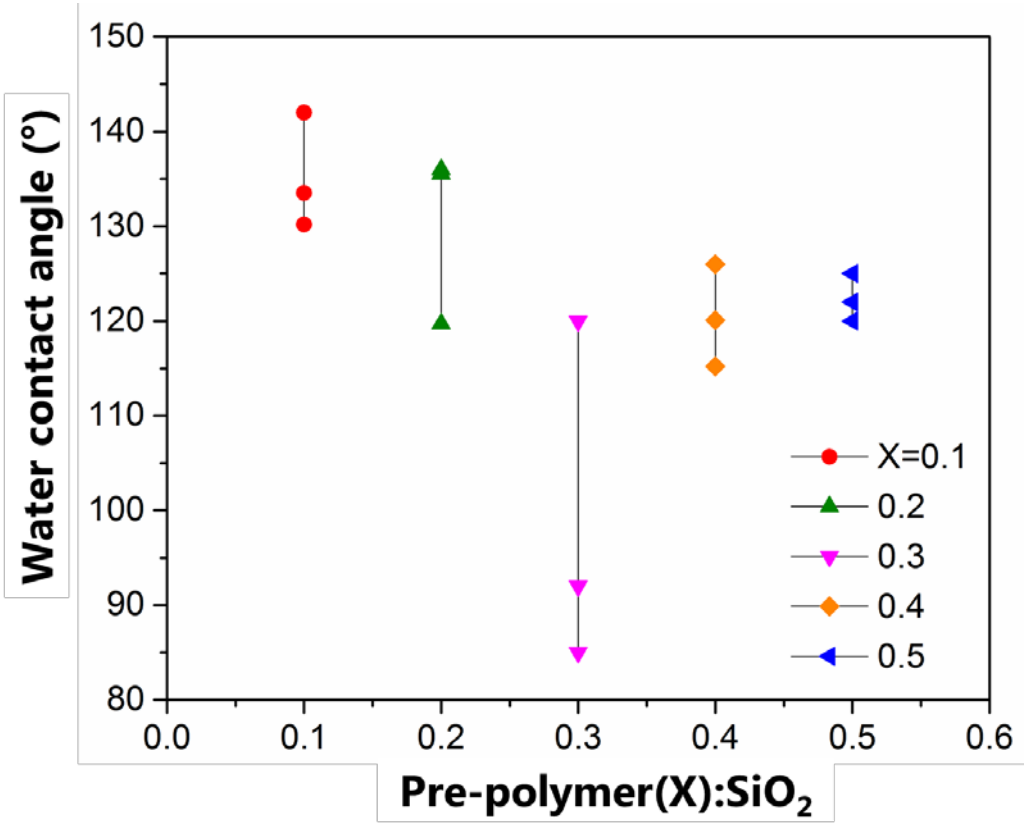

Figure S29. Water contact angles of STP-E 15 hybrid aerogels for increasing concentrations.

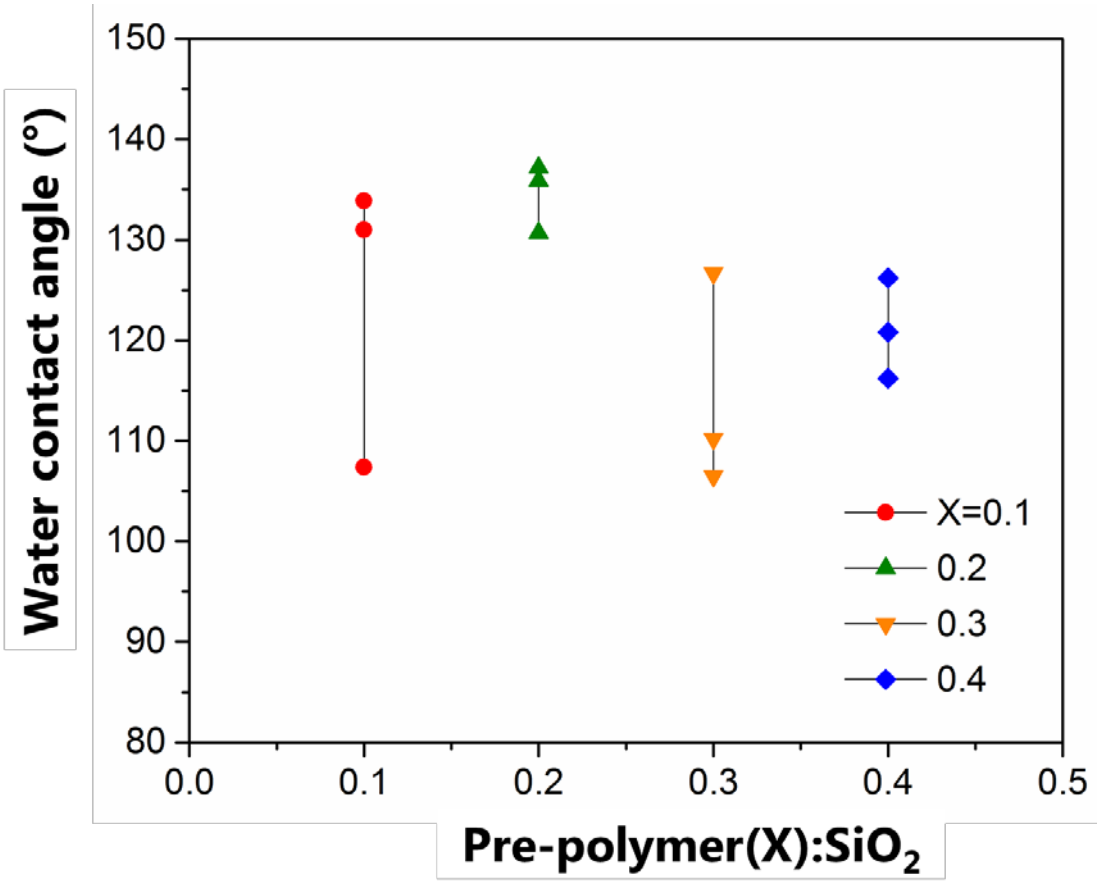

Figure S30. Water contact angles of STP-E 35 hybrid aerogels for increasing concentrations.

16. Summary of different properties of hybrid aerogels

Table S3: Summary of different properties of hybrid aerogels.

Sample	Prepolymer (X):SiO_2	ρ_{bulk} [a)] (g/cm^3)	$\rho_{skeletal}$ [b)] (g/cm^3)	S_{BET} [c)] (m^2/g)	$V_{pore,\ BJH}$ (cm^3/g)	V_{pore} [d)] (cm^3/g)	$D_{pore,\ BJH}$ (nm)	D_{pore} [e)] (nm)	λ [f)] ($mW \cdot m^{-1} \cdot K^{-1}$)	E_{mod} (MPa)	σ_{10} (MPa)	σ_{50} (MPa)	σ_{max} (MPa)	Strain at σ_{max} (%)	avg. WCA (°)	Linear shrinkage (%)
Reference silica	0.0	0.087	1.56	850	3.5	10.9	12.6	51.1	16.5	0.90	0.071	-	0.3	42	138	8
EP-M 95	0.1	0.100	-	-	-	-	-	-	15.4	0.68	0.059	0.406	2.4	80	146	10
EP-M 95	0.2	0.107	-	-	-	-	-	-	15.1	0.59	0.052	0.425	5.2	80	148	10
EP-M 95	0.25	0.104	-	-	-	-	-	-	15.3	0.61	0.053	0.396	4.1	80	-	10
EP-M 95	0.3	0.106	1.43	791	3.5	8.7	13.7	44.2	14.7	0.78	0.059	0.478	6.4	80	147	10
EP-M 95	0.4	0.119	-	-	-	-	-	-	14.8	0.91	0.072	0.593	8.4	80	148	12
EP-M 95	0.5	0.125	-	-	-	-	-	-	15.0	-	-	-	-	-	141	14
EP-M 95	0.6	0.139	1.34	673	3.6	6.4	17.6	38.3	15.0	1.55	0.100	0.867	12.2	80	146	14
EP-M 95	0.7	0.145	-	-	-	-	-	-	15.2	2.00	0.132	1.090	14.7	80	136	14
EP-M 95	0.8	0.154	-	-	-	-	-	-	15.8	2.77	0.202	1.547	19.2	80	140	16
EP-M 95	1.0	0.179	1.32	650	3.8	4.8	20.5	29.7	16.8	3.37	0.251	1.916	20.5	80	122	18
STP-E 15	0.1	0.089	-	-	-	-	-	-	17.1	-	-	-	-	-	139	8
STP-E 15	0.2	0.100	-	-	-	-	-	-	17.2	-	-	-	-	-	130	10
STP-E 15	0.25	0.126	-	-	-	-	-	-	17.0	0.80	0.063	0.387	4.9	80	-	10
STP-E 15	0.3	0.117	-	666	3.8	-	16.6	-	17.3	-					100	12
STP-E 15	0.4	0.149	-	-	-	-	-	-	17.8	-	-	-	-	-	115	18
STP-E 15	0.5	0.213	-	-	-	-	-	-	20.9	-	-	-	-	-	122	24
STP-E 35	0.1	0.094	-	-	-	-	-	-	16.4	-	-	-	-	-	132	8
STP-E 35	0.2	0.102	-	-	-	-	-	-	16.8	-	-	-	-	-	135	10
STP-E 35	0.25	0.116	-	-	-	-	-	-	16.6	0.87	0.073	0.486	6.2	80	-	10
STP-E 35	0.3	0.119	-	-	-	-	-	-	17.4	-	-	-	-	-	113	12
STP-E 35	0.4	0.144	-	-	-	-	-	-	17.8	-	-	-	-	-	119	16
Empa 2033	0.1	0.102	-	-	-	-	-	-	16.5	-	-	-	-	-	-	10
Empa 2033	0.2	0.103	-	-	-	-	-	-	15.8	-	-	-	-	-	-	10
Empa 2033	0.3	0.094	-	717	3.8	-	14.7	-	16.6	0.97	0.071	0.503	6.3	80	133	12
Empa 2033	0.4	0.115	-	-	-	-	-	-	16.0	0.95	0.076	0.578	7.6	80	-	14
Empa 2033	0.6	0.113	-	-	-	-	-	-	16.5	1.38	0.092	0.744	9.8	80	-	14
Empa 2033	0.8	0.135	-	-	-	-	-	-	17.5	1.21	0.102	0.804	9.5	80	-	16
Empa 2033	1.0	0.143	-	-	-	-	-	-	18.0	-	-	-	-	-	-	16
Empa 1990	0.3	0.097	-	-	-	-	-	-	17.0	0.88	0.072	0.502	4.4	80	144	12
Empa D-140	0.3	0.088	-	-	-	-	-	-	16.9	0.70	0.054	0.375	4.6	80	137	10
Empa D-265	0.3	0.091	-	-	-	-	-	-	17.0	0.92	0.066	0.495	4.2	80	138	10
Empa D-290	0.3	0.098	-	-	-	-	-	-	16.3	0.73	0.058	0.457	3.6	80	143	10

Estimated uncertainties: [a)] Bulk density, 5% relative; [b)] Skeletal density, 5% relative; [c)] S_{BET}, around 10 m^2/g; [d)] $V_{pore} = (1/\rho_{bulk} - 1/\rho_{skeletal})$, 10% relative; [e)] $D_{pore} = (4V_{pore}/S_{BET})$, 10% relative; [f)] Thermal conductivity, 2% relative.

17. References

[1] T. Stahl, S. Brunner, M. Zimmermann, K. Ghazi Wakili, Thermo-hygric properties of a newly developed aerogel based insulation rendering for both exterior and interior applications, Energy Build. 44 (2012) 114–117. doi:10.1016/j.enbuild.2011.09.041.

[2] L.-S. Teo, C.-Y. Chen, J.-F. Kuo, Fourier Transform Infrared Spectroscopy Study on Effects of Temperature on Hydrogen Bonding in Amine-Containing Polyurethanes and Poly(urethane−urea)s, Macromolecules. 30 (1997) 1793–1799. doi:10.1021/ma961035f.

[3] T. Ramanathan, F.T. Fisher, R.S. Ruoff, L.C. Brinson, Amino-Functionalized Carbon Nanotubes for Binding to Polymers and Biological Systems, Chem. Mater. 17 (2005) 1290–1295.

[4] C. Rudaz, R. Courson, L. Bonnet, S. Calas-Etienne, H. Sallée, T. Budtova, Aeropectin: Fully biomass-based mechanically strong and thermal superinsulating aerogel, Biomacromolecules. 15 (2014) 2188–2195. doi:10.1021/bm500345u.

[5] R. Sescousse, R. Gavillon, T. Budtova, Aerocellulose from cellulose-ionic liquid solutions: Preparation, properties and comparison with cellulose-NaOH and cellulose-NMMO routes, Carbohydr. Polym. 83 (2011) 1766–1774. doi:10.1016/j.carbpol.2010.10.043.

[6] S. Zhao, Z. Zhang, G. Sèbe, R. Wu, R. V. Rivera Virtudazo, P. Tingaut, M.M. Koebel, Multiscale assembly of superinsulating silica aerogels within silylated nanocellulosic scaffolds: Improved mechanical properties promoted by nanoscale chemical compatibilization, Adv. Funct. Mater. 25 (2015) 2326–2334. doi:10.1002/adfm.201404368.

[7] J. Cai, S. Liu, J. Feng, S. Kimura, M. Wada, S. Kuga, L. Zhang, Cellulose-silica nanocomposite aerogels by in-situ formation of silica in cellulose gel, Angew. Chemie - Int. Ed. 51 (2012) 2076–2079. doi:10.1002/anie.201105730.

[8] A. Demilecamps, C. Beauger, C. Hildenbrand, A. Rigacci, T. Budtova, Cellulose-silica aerogels, Carbohydr. Polym. 122 (2015) 293–300. doi:10.1016/j.carbpol.2015.01.022.

[9] C. Chidambareswarapattar, P.M. McCarver, H. Luo, H. Lu, C. Sotiriou-Leventis, N. Leventis, Fractal multiscale nanoporous polyurethanes: Flexible to extremely rigid aerogels from multifunctional small molecules, Chem. Mater. 25 (2013) 3205–3224. doi:10.1021/cm401623h.

[10] N. Diascorn, S. Calas, H. Sallée, P. Achard, A. Rigacci, Polyurethane aerogels synthesis for thermal insulation - textural, thermal and mechanical properties, J. Supercrit. Fluids. 106 (2015) 76–84. doi:10.1016/j.supflu.2015.05.012.

[11] A. Katti, N. Shimpi, S. Roy, H. Lu, E.F. Fabrizio, A. Dass, L.A. Capadona, N. Leventis, Chemical, Physical, and Mechanical Characterization of Isocyanate Cross-linked Amine-Modified Silica Aerogels, Chem. Mater. 18 (2006) 285–296. doi:10.1021/cm0513841.

[12] G. Churu, B. Zupančič, D. Mohite, C. Wisner, H. Luo, I. Emri, C. Sotiriou-Leventis, N. Leventis, H. Lu, Synthesis and mechanical characterization of mechanically strong, polyurea-crosslinked, ordered mesoporous silica aerogels, J. Sol-Gel Sci. Technol. 75 (2015) 98–123. doi:10.1007/s10971-015-3681-9.

[13] K.-J. Chang, Y.-Z. Wang, K.-C. Peng, H.-S. Tsai, J.-R. Chen, C.-T. Huang, K.-S. Ho,

W.-F. Lien, Preparation of silica aerogel/polyurethane composites for the application of thermal insulation, J. Polym. Res. 21 (2014) 338. doi:10.1007/s10965-013-0338-7.
[14] M.A.B. Meador, L.A. Capadona, L. McCorkle, D.S. Papadopoulos, N. Leventis, Structure−Property Relationships in Porous 3D Nanostructures as a Function of Preparation Conditions: Isocyanate Cross-Linked Silica Aerogels, Chem. Mater. 19 (2007) 2247–2260. doi:10.1021/cm070102p.
[15] S. Zhao, W.J. Malfait, A. Demilecamps, Y. Zhang, S. Brunner, L. Huber, P. Tingaut, A. Rigacci, T. Budtova, M.M. Koebel, Strong, Thermally Superinsulating Biopolymer-Silica Aerogel Hybrids by Cogelation of Silicic Acid with Pectin, Angew. Chemie - Int. Ed. 54 (2015) 14282–14286. doi:10.1002/anie.201507328.
[16] J.C.H. Wong, H. Kaymak, S. Brunner, M.M. Koebel, Mechanical properties of monolithic silica aerogels made from polyethoxydisiloxanes, Microporous Mesoporous Mater. 183 (2014) 23–29. doi:10.1016/j.micromeso.2013.08.029.
[17] P.B. Sarawade, J.-K. Kim, H.-K. Kim, H.-T. Kim, High specific surface area TEOS-based aerogels with large pore volume prepared at an ambient pressure, Appl. Surf. Sci. 254 (2007) 574–579. doi:10.1016/j.apsusc.2007.06.063.
[18] J. Yang, B. Li, H. Xu, Y. Li, X. Huo, Hydrophobicity and Phase Changes of Pd / SiO2 Organic-inorganic Hybrid Materials Calcined in Air Atmosphere Experimental, J. Fiber Bioeng. Informatics. 7:1 (2014) 117–127. doi:10.3993/jfbi03201410.